Distinguishing cancerous from noncancerous cells through analysis of electrical noise

D. C. Lovelady, T. C. Richmond, A. N. Maggi, C.-M. Lo, and D. A. Rabson*
Department of Physics, University of South Florida, Tampa, Florida 33620, USA
(Received 28 July 2007; published 11 October 2007)

Since 1984, electric cell-substrate impedance sensing (ECIS) has been used to monitor cell behavior in tissue culture and has proven sensitive to cell morphological changes and cell motility. We have taken ECIS measurements on several cultures of noncancerous and cancerous human ovarian surface epithelial cells. By analyzing the noise in real and imaginary electrical impedance, we demonstrate that it is possible to distinguish the two cell types purely from the signatures of their electrical noise. Our measures include power-spectral exponents, Hurst and detrended fluctuation analysis, and estimates of correlation time; principal-component analysis combines all the measures. The noise from both cancerous and noncancerous cultures shows correlations on many time scales, but these correlations are stronger for the noncancerous cells.

DOI: 10.1103/PhysRevE.76.041908 PACS number(s): 87.18.Ed, 87.80.Tq, 05.40.Ca

I. INTRODUCTION

Electrical cell-substrate impedance sensing (ECIS) has been in use since 1984 [1] to monitor changes in cell cultures due to spreading or in response to chemical stimuli, infection, or flow. Applications include studies of cell migration, barrier function, toxicology, angiogenesis, and apoptosis. Several papers have noted that impedance fluctuations are associated with cellular micromotion [2]. However, we are not aware of any previous work applying statistical techniques to these fluctuations in order to distinguish two different cell types. Here, we demonstrate that measures of the electrical noise from cultures of cancerous and noncancerous human ovarian surface epithelial cells distinguish them. We find that the noise in both cancerous and noncancerous cultures shows correlations on many time scales, but, by all measures, these correlations are weaker or of shorter duration in the cancerous cultures.

II. EXPERIMENTAL METHODS

We used the ECIS system to collect micromotion time-series data, the fluctuations in which are caused by the movements in a confluent layer of live cells. The system can be modeled as a RC circuit [3–6]. The cells are cultured on a small gold electrode (5×10^{-4} cm^2), which is connected in series to a 1-MΩ resister, an ac signal generator operating at 1 V and 4000 Hz, and finally to a large gold counterelectrode (0.15 cm^2). This network is connected in parallel to a lock-in amplifier, and the in-phase and out-of-phase voltages are collected once a second, from which measurement we extract time series of resistance and capacitive reactance [Fig. 1(a)]. In ECIS experiments, the fluctuations in complex impedance come primarily from changes in intercellular gaps and in the narrow spaces between the cells and the small gold electrode [4–6]. A current of about 1 μA is driven through the sample, and the resulting voltage drop of a few millivolts across the cell layer has no physiological effect: this is a noninvasive, *in vitro* technique. The cell lines used were an ovarian cancer line [Sloan-Kettering ovarian (SKOV3)] and a normal human ovarian surface epithelial (HOSE) cell line (HOSE15). These cells were grown in M199 and MCDB 105 (1:1) (Sigma, St. Louis, MO) supplemented with 10% fetal calf serum (Sigma), 2 mM *L*-glutamine, 100 units/ml penicillin, and 100 μg/ml streptomycin under 5% CO_2, and a 37 °C, high-humidity atmosphere. For ECIS micromotion measurements, cells were taken from slightly subconfluent cultures 48 h after passage, and a monodisperse cell suspension was prepared using standard tissue-culture techniques with trypsin-EDTA. These suspensions were equilibrated at incubator conditions before addition to the ECIS electrode wells. Confluent layers were formed 24 h after inoculation, resulting in a density of 10^5 cell/cm^2.

Figure 1(a) shows a representative 4096-s run (just over 1 h) measuring the real part of the impedance as a function of time; the example shows a HOSE culture, but, to the eye, SKOV cultures do not appear very different. While the example shows increasing resistance with time, others show a decrease; at this time scale; there is no evidence for an overall trend. We collected, under similar conditions, 18 time series for HOSE cultures, of which 16 went for 8192 s and two for 4096 s. Each 8192-s run was split into two halves, so that effectively we had 34 4096-s runs; however, where appropriate in the analysis below, we discard the second halves of the longer runs in order to avoid inadvertently introducing correlations. Similarly, for SKOV cultures we took data in eight 8192-s runs and ten 4096-s runs, yielding effectively 26 4096-s runs. We numerically differentiated the resistance and capacitance time series to obtain noise time series for each, which we normalized to zero mean and unit variance [Fig. 1(b)].

III. STATISTICAL MEASURES OF NOISE

We seek information from the normalized noise series. The first question to pose is whether the noise can distinguish cancerous from noncancerous cultures, but more generally the measures we extract may be used to test models of cell micromotion. Broadly, such models may be character-

*Corresponding author. davidra@ewald.cas.usf.edu

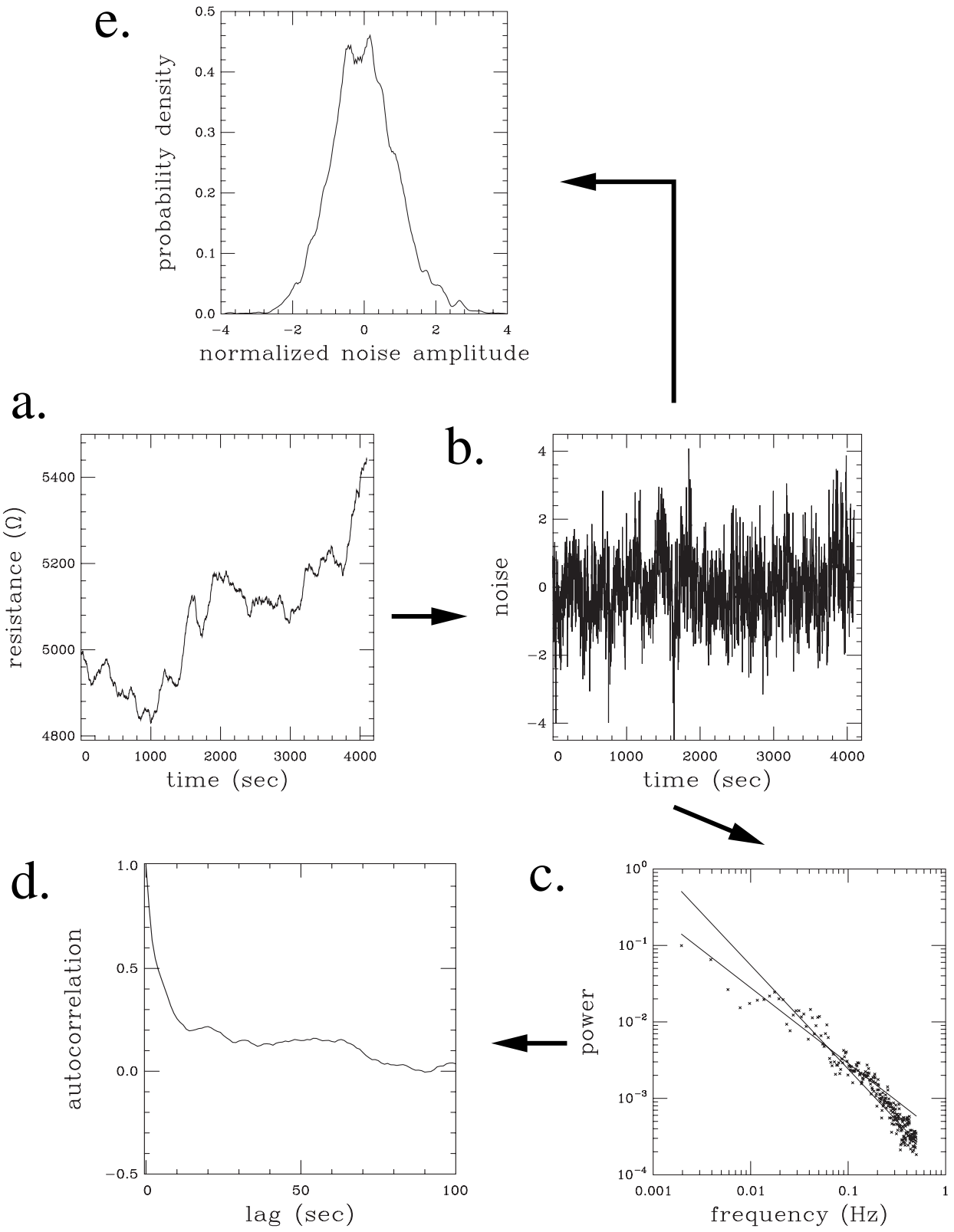

FIG. 1. Scheme of data extraction from noise. (a) Time series of resistance for one of the experimental runs. Taking the discrete-time derivative and normalizing to zero mean and unit variance gives the noise, shown in (b). The power spectrum of noise is shown in (c), using half-overlapping windows of 512 points in order to reduce scatter. Fits to the first and last 100 frequencies estimate low- and high-frequency power laws $f^{-\alpha}$. White noise would have appeared frequency independent (α=0). The Fourier transform of the power spectrum gives the autocorrelation (d), which we fitted to a shifted power-law decay to extract the measure β_0. As explained in the text, subtle differences in the univariate noise distribution (e) (smoothed) discriminate between cancerous and noncancerous micromotion.

TABLE I. Power-spectral measures of HOSE (noncancerous) and SKOV (cancerous) resistive and capacitive noise series. Shown are estimates for $1/f^{\alpha}$ behavior at high and low frequencies. The means of the α values differ by many standard errors ($\sigma/\sqrt{N}$, where σ is the standard deviation), allowing us to distinguish the populations composed of N runs, although not by enough to distinguish reliably a *single* HOSE run from a *single* SKOV. The F test and t test give the probabilities that the variances and means of the distributions of values of α would differ by as much as or more than they do if the two populations had come from the same Gaussian distribution. KS gives the probability under the Kolmogorov-Smirnov test that the two populations' cumulative distributions could differ as much as they do. Small probabilities indicate that the populations differ; a probability of 0 means $<10^{-6}$. $N=34$ for HOSE, $N=26$ for SKOV. In all cases, we apply the approximate t test for distributions with unequal variances [7].

	HOSE			SKOV			Probability from same distribution		
Measure	Average	σ	$\sigma/\sqrt{N}$	Average	σ	$\sigma/\sqrt{N}$	F test	t test	KS test
				Resistance					
α_{low}	0.991	0.132	0.02	0.800	0.148	0.03	0.54	$4.\times10^{-6}$	4.2×10^{-4}
α_{high}	1.58	0.558	0.10	1.09	0.648	0.13	0.42	$4.\times10^{-3}$	0.024
				Capacitance					
α_{low}	0.909	0.0988	0.02	0.734	0.131	0.03	0.13	0	$9.\times10^{-6}$
α_{high}	1.133	0.446	0.08	0.980	0.357	0.07	0.25	0.15	0.37

ized by short- and long-term correlation, so we look at several measures for each.

First, the power spectral density [Fig. 1(c)] looks very much more like "pink noise" than "white noise;" that is, it shows signs of long-time correlations. A log-log plot of spectral density against frequency f suggests an intensity varying as $f^{-\alpha}$ in the low-frequency limit. (We discuss below the extent to which a true white-noise process may mimic pink noise due to the finite time of a run.) For each run, we split the 4096 noise amplitudes into half-overlapping windows of 512 s, multiplied by a Hann window, Fourier transformed, and squared, averaging the resulting spectra in order to reduce scatter [7].

As in the example of the figure, some runs show a crossover between low- and high-frequency values for α, which we estimated with least-squares straight-line fits of power at the first 100 (excluding zero frequency and the very lowest frequency) and last 100 frequencies (out of 256 nonzero frequencies). In many runs, low- and high-frequency α estimates were equal, within fitting errors. Table I summarizes the results, giving in the columns labeled "Average" the means over all HOSE runs or all SKOV runs for the given measures; the columns labeled "σ" give the standard-deviation estimator for the population of all like runs. The differences between α values for HOSE and SKOV, both low and high frequency, exceed several standard errors (or standard deviations of the mean, $\sigma/\sqrt{N}$, where σ is the standard deviation and N is the number of runs). Moreover, the Student t test and Kolmogorov-Smirnov test show that the HOSE and SKOV populations differ.[1] The low-frequency exponents are more significant. The fact that these measures are larger for HOSE than for SKOV suggests a difference in long-time correlations in micromotion and is consistent with the hypothesis that noncancerous HOSE cells move in a more orderly manner than cancerous SKOV cells.

A nonzero α_{low} is indicative of long-time, "fractal" [8], correlation, but as Rangarajan and Ding [9] point out, relying on power-law behavior alone can lead to incorrect identification of such correlations when none exist. Two related measures are the Hurst exponent and the exponent of detrended fluctuation analysis [8,10–14]; both methods split the time series of noise into bins of duration T, then determine how a measure scales with T. For the Hurst exponent, one subtracts the mean from all the data in a bin and characterizes that bin by its standard deviation S. The series is integrated, and the minimum value subtracted from the maximum, yielding the range R. For each bin, one records the ratio R/S and averages over bins of the same size. The procedure is repeated for successively larger bins (T). A straight-line fit to a log-log plot of R/S against bin size T reveals a power law, $R/S \sim T^{H}$, where H is the Hurst exponent. Detrended fluctuation analysis (DFA) runs along similar lines, but within each bin one subtracts a best-fit line, thus detrending the data. The data in the bin are then characterized by standard deviation $S \sim T^{D}$, where D is the DFA exponent. Table II shows the results; again, with high confidence (based particularly on Student's t test), we can conclude that HOSE and SKOV noise come from different distributions. However, since the means are separated by less than a population standard deviation, many runs (of 4096 s) would be necessary to determine the provenance of *one* particular culture.

While α_{low}, H, and D were designed to estimate correlations at diverging time scales, short-time correlation is conveniently determined from autocorrelation, Fig. 1(d), normalized to unity at zero lag. The lag of the first zero crossing provides one natural measure of when correlation is lost, but since autocorrelation curves may sometimes reach very small, yet positive, plateaus before crossing zero, we also measured the lag at which the autocorrelation first crosses $1/e$. In a model with only short-time correlation, the $1/e$

[1]Typically, the Kolmogorov-Smirnov test is taken to reject the (null) hypothesis that two populations were drawn from the same distribution if it yields a probability less than 5%. Three of the four α measures meet this criterion. As a control test, half of the HOSE runs were checked against the other half and SKOV against SKOV, and in every case the α measurements were compatible with the null hypothesis, as expected.

TABLE II. Additional measures of long-time correlation in the noise time series, Hurst and detrended-fluctuation exponents. See Table I caption for column descriptions.

	HOSE			SKOV			Probability from same distribution		
Measure	Average	σ	$\sigma/\sqrt{N}$	Average	σ	$\sigma/\sqrt{N}$	F test	t test	KS test
				Resistance					
Hurst H	0.770	0.0442	0.008	0.744	0.0876	0.017	$3.\times10^{-4}$	0.17	0.099
DFA D	0.854	0.0473	0.008	0.806	0.0793	0.016	0.006	9.8×10^{-3}	0.057
				Capacitance					
Hurst H	0.792	0.0474	0.008	0.731	0.0886	0.017	$9.\times10^{-4}$	3.1×10^{-3}	0.012
DFA D	0.843	0.0479	0.008	0.788	0.0748	0.015	0.017	2.5×10^{-3}	3.4×10^{-3}

time estimates the exponential decay time. However, as we discuss below, we observed significant deviations from exponential decay, finding better fits to a shifted power-law decay,

$$(\text{autocorrelation}) = \left(\frac{t+t_1}{t_1}\right)^{-\beta_0}. \quad (1)$$

We fitted autocorrelation, for lags in the heuristic interval $t=1-20$ s, using Levenberg-Marquardt least-squares minimization to this form to find β_0. Table III summarizes results for the two crossings and β_0; the last distinguishes the populations of HOSE and SKOV runs only in that the (cancerous) SKOV population shows much greater scatter in β_0, as measured by the F test. Both crossings vary greatly from run to run, but the $1/e$ crossing in resistance and zero crossing in capacitance distinguish the populations of HOSE and SKOV experiments at better than the 95% confidence level as measured by Student's t test and the Kolmogorov-Smirnov test. In particular, the averaged measures show shorter crossing times and steeper descents (β_0) for SKOV than for HOSE, again consistent with the hypothesis that the micromotion of cancerous cultures is less correlated than that of noncancerous cultures.

With the 14 measures summarized in Tables I–III, each run of 4096 s can be thought of as a point in a 14-dimensional space. In such problems, the populations might separate into two distinct, compact clusters ([15] Sec. 4.2); while the identification of clusters in high-dimensional spaces remains an open problem in statistical research, it is common to use the variance-maximizing principal-component analysis introduced by Hotelling to project onto optimal subspaces, usually taken to be two dimensional [16]. Figure 2 plots the first two principal components. While the plot shows a clear difference between the two populations consisting of all runs of HOSE and all runs of SKOV, overlap between the two clusters makes it difficult to apply the technique diagnostically. We found this problem to be generic: an exhaustive examination of pairs of principal components (beyond the first two) produced similar plots, with the two populations usually less distinct in higher-order components, while adding or subtracting several measures to the list of 14 measures did not improve clustering.

Thus far, the noise measures considered have shown that electrical noise from HOSE and SKOV experiments have, on average, different correlations, but they do not provide a reliable way to determine whether the cells in a single run of 4096 s are HOSE or SKOV. However, from the normalized

TABLE III. Measures of short-time correlation in the noise time series: the lag at which normalized autocorrelation [see Fig. 1(d)] falls to $1/e$, the first zero crossing of autocorrelation, and the exponent β_0 from fitting the first few lags with a shifted power law. See the Table I caption for the statistical labels. Of these measures, the $1/e$ crossing (in resistance) and the zero crossing (in capacitance) have the greatest significance in distinguishing the populations; β_0 is significant only in the sense that the *scatter* is very much greater for cancerous SKOV than for noncancerous HOSE.

	HOSE			SKOV			Probability from same distribution		
Measure	Average	σ	$\sigma/\sqrt{N}$	Average	σ	$\sigma/\sqrt{N}$	F test	t test	KS test
				Resistance					
$1/e$	6.35	1.76	0.30	4.91	2.62	0.51	0.032	0.020	9.1×10^{-3}
Zero	132	88.0	15	111	115	23	0.14	0.44	0.068
β_0	1.18	0.565	0.10	5.11	12.8	2.50	0.	0.13	0.48
				Capacitance					
$1/e$	5.77	1.40	0.24	4.40	3.96	0.78	0.	0.10	6.0×10^{-5}
Zero	194	136	23	97.5	111	22	0.29	3.7×10^{-3}	8.6×10^{-3}
β_0	1.17	1.16	0.20	1.93	3.35	0.66	0.	0.28	0.71

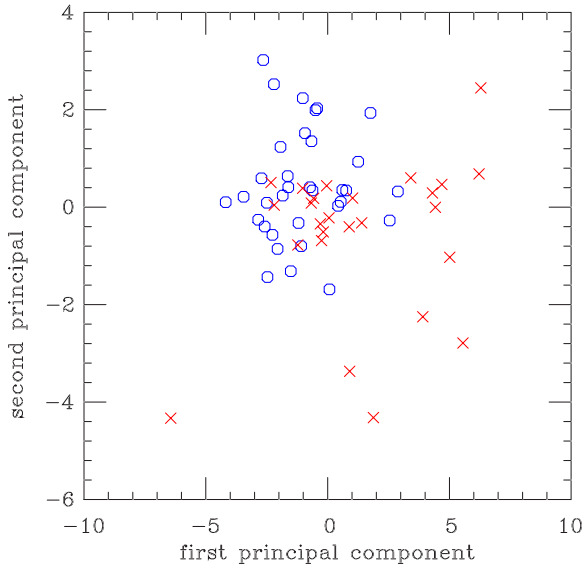

FIG. 2. (Color online) Projection along the first two principal components of the 14-dimensional space determined by Tables I–III. Blue open symbols mark the 34 HOSE runs, red crosses the 26 SKOV experiments. As populations, these two sets are distinct, but the overlap of clusters makes it difficult to distinguish individual runs in this type of projection.

(zero-mean, unit-variance) noise time series of Fig. 1(b), we can extract a probability distribution of noise amplitudes, as in Fig. 1(e). Not surprisingly, the distribution is approximately Gaussian; however, subtle deviations from normal form do distinguish HOSE from SKOV populations, even in a single run, if we apply the Kolmogorov-Smirnov test directly to the noise. This test looks only at distributions of noise amplitudes, rather than correlations.

To this end, we concatenate the first nine 4096-s HOSE resistance runs (discarding, for this purpose, the second halves of the 8192-s runs) to create a HOSE resistance reference distribution. Similarly, we create a SKOV resistance reference by concatenating the first nine 4096-s SKOV runs. Each of the remaining runs is tested against the two resistance reference sets. The same procedure is applied with capacitance data. In many cases, the Kolmogorov-Smirnov test does not show a match with either distribution with high probability, but we can compare the two probabilities: one typical HOSE run matches the HOSE reference with probability 0.02 and SKOV with probability 4.7×10^{-8}, so we (correctly) identify this run as HOSE based on the ratio of probabilities. Of 56 tested data sets (none of which went into the construction of the reference sets), 42 (75%) matched the correct reference set by this criterion, an outcome that would happen by chance with probability approximately 1.2×10^{-4}. We repeated the procedure using a second collection of four reference sets (HOSE and SKOV, resistance and capacitance) each constructed from nine runs not used in making the first reference sets. Of 64 trials (none used in the new reference sets), 53 (83%) were identified correctly, with corresponding probability 5×10^{-8}. The results from the two sets of trials are added and summarized in Table IV. We can reduce percentages of incorrect identifications by insisting on agreement between resistance and capacitance time series; this lowers the overall incorrect identification rate to 11.7%, with a correct rate of 70.0% and a "not sure" rate of 18.3%.

TABLE IV. Percentages of correct identifications. The Kolmogorov-Smirnov test is applied to distributions of noise amplitudes against HOSE and SKOV reference sets. Two nonoverlapping choices of reference sets are used; in neither case did any trial run figure in a reference set against which it was tested. The "average" column gives percentages weighted by numbers of trials (16 HOSE and 12 SKOV in the first set, 18 HOSE and 14 SKOV in the second).

	First set	Second set	Average
HOSE capacitance	62.5%	72.2%	67.6%
HOSE resistance	87.5	66.7	76.5
SKOV capacitance	83.3	100	92.3
SKOV resistance	66.7	100	84.6
All resistance	78.6	81.3	80.0
All capacitance	71.4	84.4	78.3
All HOSE	75.0	69.4	72.1
All SKOV	75.0	100	88.5
All	75.0	82.8	79.2

Viewed by eye, the kernel-smoothed probability distribution function of a noise time series looks approximately normal (Gaussian), although often with outliers; see Fig. 1(e). Deviations from normality are characterized in part by kurtosis,[2] which is larger for HOSE than for SKOV: see Table V. A possible explanation is that kurtosis here is a proxy for correlation. Under this hypothesis, two effects could be at work. First, while all of our runs have the same number of time steps, Table III shows that SKOV correlation times are shorter than HOSE correlation times; thus, a SKOV run could be said to have more *independent* time steps than a HOSE run of the same length. The standard deviation of the estimator of kurtosis scales as $1/\sqrt{N}$, with N the number of independent samples [22]. The ratios of 18 in Table V between standard deviations of kurtoses from the populations of all HOSE and all SKOV imply much too large a ratio of correlation times (18^2), but qualitatively they support the idea of more independent samples in the SKOV population. However, this first effect would not result in the observed statistically significant differences in mean kurtoses. A second possible manifestation of correlation gets to the heart of why the noise distributions appear approximately Gaussian: a large number of cells contribute to the overall measurement of resistance or capacitance. We would expect a normal distribution in the limit of infinitely many cells; however, convergence under the central-limit theorem is nonuniform, with a distribution approaching a Gaussian slowly in the tails as the number of independent cellular motions increases. If, as we believe, HOSE motion is more

[2]Conventions for kurtosis abound. Specifically, we mean the unbiased estimator $g_2=k_4/k_2^2$, where k_i are the Fisher statistics: (see [22]). Since the quantity estimated by g_2 is zero for a normal distribution, it is sometimes referred to as "kurtosis excess."

TABLE V. Kurtosis averaged over all runs, standard deviation of kurtoses, and standard deviation of the means. *F*-test probabilities for HOSE and SKOV to come from the same distribution were both $<10^{-6}$; *t*-test probabilities were 0.022 for resistance and 0.005 for capacitance. The Kolmogorov-Smirnov test gave probability $<10^{-6}$ for resistance and 6×10^{-5} for capacitance.

	Average	σ	$\sigma/\sqrt{N}$
HOSE resistance	74.4	173.1	29.7
SKOV resistance	3.00	9.57	1.9
HOSE capacitance	17.6	32.2	5.5
SKOV capacitance	0.94	1.80	0.35

correlated than SKOV, it would comprise *fewer* independent cellular motions and so have a larger kurtosis.

Temporal correlation cannot explain the whole effect: as we argue in Appendix A, both kurtosis and the Kolmogorov-Smirnov test appear to be better discriminants than a direct measure, the $1/e$ crossing. This suggests that the univariate noise distribution is more than just a proxy for correlation time. In Appendix B, we consider whether the observed kurtosis could result from spatial correlations[3] proportional to the measured temporal correlations and argue that the kurtosis effect is too strong and the coupling between kurtosis and temporal correlation too weak to support this hypothesis.

IV. TWO SIMPLE MODELS

Having motivated and interpreted our measures of noise in terms of short- and long-time correlations, we now compare our data to the simplest possible discrete-time models, the binary random walk with persistence [17], displaying only short-time correlation, and a discrete fractional Brownian motion [9,18], which has correlations on all time scales. For present purposes, it suffices to consider only the increments rather than the walks themselves; that is, we compare to Fig. 1(b), not Fig. 1(a).

First, consider the increments of a discrete random walk with persistence. Let the increment at time $j\Delta t$, where Δt is the time step, be x_j, drawn from $\{+1,-1\}$. Then $x_{j+1}=x_j$ with probability a and $x_{j+1}=-x_j$ with probability $1-a$; one recovers the usual discrete binary random walk for $a=1/2$. Since we think of this process as approximating a continuous one, and there is no natural way to take the limit $\Delta t\to0$ for anticorrelated increments, we restrict a to $1/2\le a\le1$. For convenience, we set $\Delta t=1$. A simple inductive argument shows that

$$\langle x_0x_n\rangle=(2a-1)^n=\exp(-n/\tau), \tag{2}$$

where the correlation time $\tau=-1/\ln(2a-1)$. For times much larger than τ, this Markov process looks like an ordinary binary random walk with a rescaled time, and by the usual arguments [19], the power spectrum approaches white noise, i.e., it becomes independent of frequency in the low-frequency limit. However, for a finite run, the power spectrum may mimic correlated (pink) noise even, surprisingly, for a τ as short as 4 in a run as long as 4096 s, as in Fig. 3(a). However, the random noise levels off noticeably at low frequencies, while the experimental data [Fig. 3(b)] appear to follow a $1/f^\alpha$ power law to the lowest frequencies.[4] This supports the presence of correlations at all time scales. The shortness of the low-frequency plateau in Fig. 3(a) is misleading. To see more of the flat part of the spectrum, finer frequency resolution is necessary. Taking larger windows, we can (at least for a run longer than 4096 s) extend the graph many decades to the left and verify that the spectrum remains flat (white), but at the cost of greater scatter. Figures 3(c) and 3(d) show autocorrelation for random noise and experimental data with fits to exponential decay (dotted) and the shifted power law (1) (solid). The two fits fall on top of one another for the process satisfying (2). That exponential decay does not approximate the experimental data as well as the power law corroborates the hypothesis of longer-than-short-time correlations.

Mandelbrot and van Ness [18] introduce the notion of fractional Brownian motion with correlations between increments separated by arbitrary time differences and with a $1/f^\alpha$ power spectrum. Rangarajan and Ding [9] describe a particularly simple way of generating a time series of increments with such properties: start with a Gaussian-distributed uncorrelated time series $\{x_j\}$, Fourier transform, multiply by $f^{-\alpha/2}$, and Fourier transform back. The resulting process has a Hurst exponent given by

$$H=(1+\alpha)/2. \tag{3}$$

Determination of the exponents α and H is subject to the usual numerical vicissitudes, but Rangarajan and Ding argue that true long-ranged processes should satisfy (3) at least approximately.

Figure 4 plots fractional discrepancies between (3) and measured Hurst exponents as functions of measured spectral exponents α. At the bottom are plotted artificially generated long-time-correlated data following the prescription of Rangarajan and Ding (plotting symbols +); the measured exponents α are always close to the known values, so the measurement errors occur in estimating H. We note a systematic trend toward larger errors away from $\alpha\approx0.5$, but generally the errors stay small. At the top of the graph (plotting symbols $\diamond$) are artificially generated random-walk increments with persistence times ranging from 2 at the left to 7 at the right. Measured values of α follow the same prescription as used above, although as noted earlier (Fig. 3), the fits fail for low frequencies; indeed, every α should be zero. Hurst estimates range from 0.45 to 0.67; the true value in every case should be 1/2. As discussed by Rangarajan and Ding, the discrepancies between measured Hurst exponents and those estimated from measured α are large. In the middle and at the bottom are plotted our experimental data (HOSE $\circ$; SKOV $\times$). Agreement between the exponents H and α is

[3] We will report elsewhere on direct measures of spatial correlation in micromotion.

[4] Indeed, our Fig. 3(a) resembles Fig. 6(b) of Ref. [9]. That process also has no true long-time correlations.

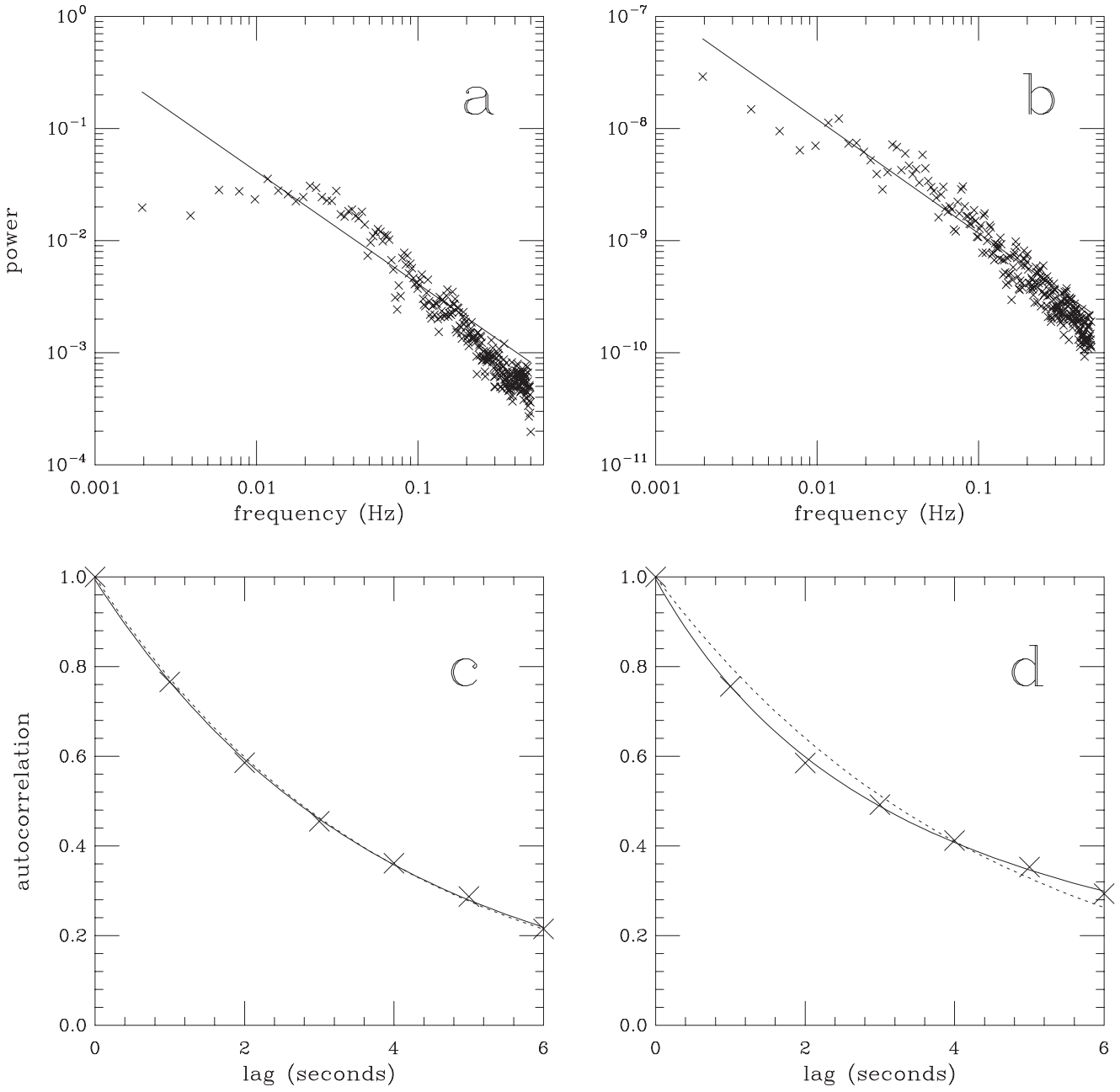

FIG. 3. Increments of a finite random walk with persistence (left) may mimic certain aspects of the experimental data (right), but with notable differences. The random process has $a=0.8894$, so an exponential decay time $\tau=4.00$. The experiment is a typical capacitance-noise time series of HOSE, with a measured $1/e$ crossing of 5.7. (a) and (b) show the best-fit lines to the first 100 points (excluding zero and the lowest frequency) of the power spectrum; both give slopes ≈ -1.0, but the random data level off noticeably at low frequencies, as would be expected of white noise. Autocorrelation curves (c) and (d) show fits to exponential (dotted line) and shifted power-law (1) (solid) decays. For the random noise, the two fits fall on top of one another, but for the experimental data, a power law fits better than exponential decay.

generally not as good as for the long-range-correlated processes but not so poor as for the short-time-correlated random walk. On average, the experimental points lie closer to the former than to the latter. We interpret this result as supporting the existence of correlations on, at the very least, many different time scales. A model of cell motion will need to explain both the short- and long-time correlations we have observed.

V. APPLICATIONS

We have demonstrated that electrical-noise measurements on human ovarian surface epithelial cells can distinguish cancerous and noncancerous cultures. This is not intended as a diagnostic tool; for one thing, it is easier to distinguish them under a microscope. We find it is also possible to distinguish HOSE from SKOV populations based purely on *average* electrical resistance or capacitance. Our main focus

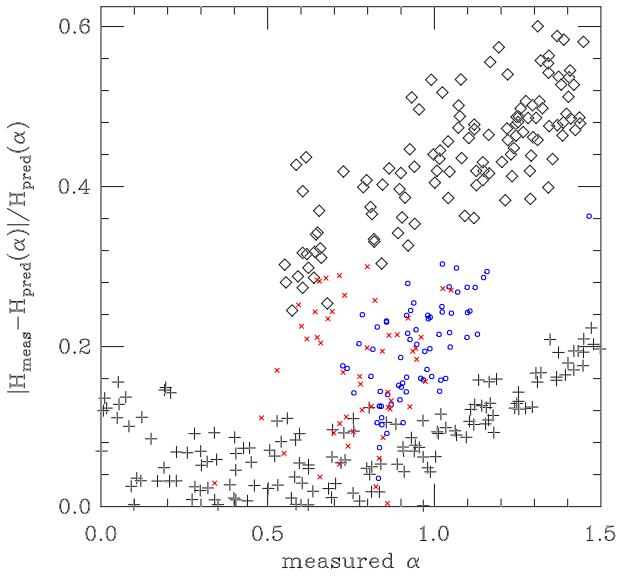

FIG. 4. (Color online) Fractional discrepancies between H_{pred} given by (3) and measured Hurst exponent as functions of measured spectral exponent α_{low}. Near the bottom, plotted with large + symbols, are artificially generated data with known long-time correlations. At top are generated data (large ◇) from random-walk increments with persistence times ranging from 2 (smaller values of α) to 7 (larger values). In the middle are experimental results for HOSE (blue ◦) and SKOV (red ×). Most of the experimental data look more like the correlated data than the uncorrelated, but a few overlap with uncorrelated noise; all of these are SKOV.

has rather been on developing statistical tools with which to test more sophisticated statistical-mechanical models and on developing a database of characteristics of many different cell types, for which a single measurement (e.g., average electrical resistance) will surely be inadequate. The application of the ECIS methodology to investigate cell motility in culture under different environmental conditions may provide a useful tool in this effort.

Motility of cells in tissue culture has been widely observed and is thought to be an expression of a basic cellular mechanism involved in numerous physiological and pathological processes, such as morphogenesis, wound healing, and tumor metastasis. In addition to locomotion, motility may take the form of membrane ruffling and undulations and the extension of regions of the cytoplasm in the form of blebs and lamellipodia. While normal cells exhibit steady control of their growth rate and motile behavior in response to cell-substrate and cell-cell interactions, the lack of such contact inhibition in cancer cells is directly responsible for their invasive behavior [20]. In an ECIS measurement, as the cells attach and spread on the electrode surface, the electric current must flow in the spaces under and between the cells, as the cell membranes are essentially insulators. In reducing the area available for current flow, this initial motion causes a large increase in impedance. This generally peaks a few hours into the experiment; our data were taken well after the peak. Subsequent smaller changes in the cell-substrate and cell-cell interactions due to cell motions cause the impedance to fluctuate with time. The numerical methods used in this paper open the way to analyzing impedance fluctuations measured by ECIS and may provide information about cellular dynamics such as different behavior between cancerous and healthy cells.

Our observation of shorter correlation times in cancerous cultures is consistent with the picture of these cells moving in a less regulated manner. Now that it has been established that different cell types generate distinguishable noise patterns, future research in this area will focus on the development of realistic models of cellular motility for healthy and malignant cells.

ACKNOWLEDGMENTS

We acknowledge the participation of Hiep Q. Le. This work was supported in part by a grant from the Florida Space Research Institute. We would also like to thank Dr. Samuel Mok at Harvard Medical School for providing us with the cell lines used in this study. Finally, we thank Heather Harper for helpful comments on the manuscript.

APPENDIX A: COMPARING DISCRIMINANTS

We claim no originality to the following elementary application of statistics but could not find a textbook discussion of quite this point. Given two distributions A and B (for instance, the kurtoses of HOSE data sets and those of SKOV), assumed to be Gaussian and characterized by means $\mu_A < \mu_B$ and standard deviations σ_A, σ_B, there are several choices of where to place a dividing point x_0 so as to identify all $x < x_0$ as belonging to population A and all $x > x_0$ to population B. One natural choice is to pick x_0 so that the expected rates of correct identification of the two populations will be the same, i.e., that $x_0 - \mu_A$ should be the same multiple of σ_A as $\mu_B - x_0$ is of σ_B, or

$$x_0 = \frac{\mu_A \sigma_B + \mu_B \sigma_A}{\sigma_A + \sigma_B}. \tag{A1}$$

Any other choice will decrease the expected rate of incorrect identification of one population at the cost of increasing the other. A second plausible choice is to seek to maximize the sum of the expected correct identification rates,

$$C_A = \frac{1}{2} + \frac{1}{2}\,\text{erf}\left(\frac{x_0 - \mu_A}{\sigma_A \sqrt{2}}\right),$$

$$C_B = \frac{1}{2} + \frac{1}{2}\,\text{erf}\left(\frac{\mu_B - x_0}{\sigma_B \sqrt{2}}\right); \tag{A2}$$

it is easy to show that the separatrix x_0 is then

$$x_0 = \frac{\mu_B\sigma_A^2 - \sigma_B[\mu_A\sigma_B \pm \sigma_A\sqrt{(\mu_A-\mu_B)^2 + 2(\sigma_A^2-\sigma_B^2)\ln(\sigma_A/\sigma_B)}]}{\sigma_A^2-\sigma_B^2}. \quad \text{(A3)}$$

[One root maximizes C_A+C_B. Note that (A3) reduces to $(\mu_A+\mu_B)/2$ when $\sigma_A=\sigma_B$.] A third natural choice, maximizing the product C_AC_B, requires numerical solution. Of course, a more complicated risk function could apply, for instance in medical diagnosis, where a false negative is much worse than a false positive.

To compare the predictive values of three of the statistical measures developed in the text, $1/e$ crossing from Table III, kurtosis from Table V, and the Kolmogorov-Smirnov test of Table IV, we apply the simplest separatrix (A1) to the means and standard deviations estimated for the first two. [This choice is motivated by the similar correct-identification percentages for HOSE and SKOV populations in Table IV, but as an alternative to (A2), using the actual data sets gives comparable answers.] Then the expected correct-identification rate (A2) for $1/e$ as a discriminant is 62% and that for kurtosis 67%. These rates are both lower than the 79% (Table IV) for the Kolmogorov-Smirnov test applied to the noise distribution, undermining the idea that the deviation of this distribution from normal form is strictly a proxy for correlation time.

APPENDIX B: KURTOSIS AND CORRELATION LENGTH

In Appendix A, we argued from the data that because $1/e$ decay time as a measure of correlation time does not discriminate HOSE cultures from SKOV as well as the Kolmogorov-Smirnov test on the noise distributions, the latter must be more than a proxy for temporal correlation. We now consider whether spatial correlation, which this experiment does not measure directly,[3] might enhance kurtosis by reducing the number of independent motions responsible for the measured time series, as discussed in Sec. III.

The resistance or capacitance measured at a given time is the result of motion involving many cells. If we view the total signal as the sum of many components, and if each of these has a nondivergent variance, the central-limit theorem holds, and we expect approximately a Gaussian distribution, which we observe [Fig. 1(e)]. As is well known, convergence under the central-limit theorem as the number of components $n\to\infty$ is nonuniform, and, for finite n, outliers can affect the kurtosis. The binomial distribution (for definiteness, with equal probabilities for individual events ±1) provides a familiar example. Here, kurtosis $\gamma_2=-2/n$ {[21], (26.1.20)}, but more generally we would expect $\gamma_2\sim n^{-1}$ for the whole class of related models. If a spatial correlation length is supposed proportional to the correlation time, τ, then we would expect $n\sim\tau^{-2}$, since the culture is two dimensional, so that

$$\gamma_2 \sim \tau^2. \quad \text{(B1)}$$

A comparison of *average* $1/e$ times from Table III, estimating τ, to average estimated kurtoses from Table V shows a monotonic increase of kurtosis with τ, as predicted. However, the increase is very much more rapid than τ^2, roughly τ^{12}, according to these four data points. The very large ratios of kurtosis between HOSE and SKOV samples (factor of 25 for resistance, 19 for capacitance) for modest increases in $1/e$ times (29% and 31%) suggest that spatial correlations are stronger than temporal ones. On the other hand, scatter plots (for resistance and for capacitance data) of kurtosis versus $1/e$ time for the 60 runs show tremendous variation and no evident trend; only on average do we see monotonic behavior. This suggests that temporal correlation and kurtosis, while both discriminants between HOSE and SKOV, may not be strongly coupled.

[1] I. Giaever and C. R. Keese, Proc. Natl. Acad. Sci. U.S.A. **81**, 3761 (1984).
[2] J. H. T. Luong, Anal. Lett. **36**, 3147 (2003).
[3] I. Giaever and C. R. Keese, Physica D **38**, 128 (1989).
[4] I. Giaever and C. R. Keese, Proc. Natl. Acad. Sci. U.S.A. **88**, 7896 (1991).
[5] C.-M. Lo, C. R. Keese, and I. Giaever, Exp. Cell Res. **204**, 102 (1993).
[6] C.-M. Lo, C. R. Keese, and I. Giaever, Biophys. J. **69**, 2800 (1995).
[7] W. H. Press, S. A. Teukolsky, W. T. Vetterling, and B. P. Flannery, *Numerical Recipes in C: The Art of Scientific Computing*, 2nd, corrected ed. (Cambridge University Press, Cambridge, U.K., 1994).
[8] J. B. Bassingthwaighte, L. S. Liebovitch, and B. J. West, *Fractal Physiology* (Oxford University Press, New York, 1994).
[9] G. Rangarajan and M. Ding, Phys. Rev. E **61**, 4991 (2000).
[10] B. B. Mandelbrot and J. R. Wallis, Water Resour. Res. **5**, 321 (1969).
[11] J. Feder, *Fractals* (Oxford University Press, New York, 1988).
[12] C.-K. Peng, S. V. Buldyrev, S. Havlin, M. Simons, H. E. Stanley, and A. L. Goldberger, Phys. Rev. E **49**, 1685 (1994).
[13] C.-K. Peng, S. Havlin, H. E. Stanley, and A. L. Goldberger, Chaos **5**, 82 (1995).
[14] A. Goldberger, A. N. Amaral, L. Glass, J. M. Hausdorff, P. Ch. Ivanov, R. G. Mark, J. E. Mietus, G. B. Moody, C.-K. Peng, and H. E. Stanley, Circulation **101**, e215 (2000).
[15] M. Lewicki, Network Comput. Neural Syst. **9**, R53 (1998).
[16] H. Hotelling, J. Educ. Psychol. **24**, 417 (1933).
[17] R. Fürth, Z. Phys. **2**, 244 (1920).

[18] B. B. Mandelbrot and J. W. van Ness, SIAM Rev. **10**, 422 (1968).
[19] L. E. Reichl, *A Modern Course in Statistical Physics*, 2nd ed. (John Wiley and Sons, New York, 1998).
[20] D. Hanahan and R. A. Weinberg, Cell **100**, 57 (2000).
[21] *Handbook of Mathematical Functions*, edited by M. Abramowitz and I. A. Stegun (Dover, New York, 1972).
[22] E. Keeping, *Introduction to Statistical Inference* (van Nostrand, Princeton, NJ, 1962; republished Dover, New York, 1995).